Electrokinetic Analysis of Cell Translocation in Low-Cost Microfluidic Cytometry for Tumor Cell Detection and Enumeration

Article *in* IEEE transactions on bio-medical engineering · August 2013

DOI: 10.1109/TBME.2013.2278014 · Source: PubMed

CITATIONS
15

READS
96

5 authors, including:

Jinhong Guo
University of Electronic Science and Technology of China
115 PUBLICATIONS **881** CITATIONS
SEE PROFILE

Tze Sian Pui
Agency for Science, Technology and Research (A*STAR)
17 PUBLICATIONS **355** CITATIONS
SEE PROFILE

Yong-Ling Ban
University of Electronic Science and Technology of China
102 PUBLICATIONS **1,355** CITATIONS
SEE PROFILE

Abdur rub abdur rahman
Agency for Science, Technology and Research (A*STAR)
29 PUBLICATIONS **666** CITATIONS
SEE PROFILE

Electrokinetic Analysis of Cell Translocation in Low-Cost Microfluidic Cytometry for Tumor Cell Detection and Enumeration

Jinhong Guo, Tze Sian Pui, Yong-Ling Ban, Abdur Rub Abdur Rahman, and Yuejun Kang*

***Abstract*—Conventional Coulter counters have been introduced as an important tool in biological cell assays since several decades ago. Recently, the emerging portable Coulter counter has demonstrated its merits in point of care diagnostics, such as on chip detection and enumeration of circulating tumor cells (CTC). The working principle is based on the cell translocation time and amplitude of electrical current change that the cell induces. In this paper, we provide an analysis of a Coulter counter that evaluates the hydrodynamic and electrokinetic properties of polystyrene microparticles in a microfluidic channel. The hydrodynamic force and electrokinetic force are concurrently analyzed to determine the translocation time and the electrical current pulses induced by the particles. Finally, we characterize the chip performance for CTC detection. The experimental results validate the numerical analysis of the microfluidic chip. The presented model can provide critical insight and guidance for developing micro-Coulter counter for point of care prognosis.**

***Index Terms*—Circulating tumor cell, Coulter counter, electrokinetic, hydrodynamic, point of care.**

I. Introduction

COULTER counter has emerged as a powerful tool for the detection and enumeration of biological particles or cells in fluidic electrolyte solution [1]. Their applications range widely from the analysis of pollen [2], human cells [3], bacteria [4], viruses [5], DNA, and other biomolecules [6], [7], to ion detection for some industrial applications. When microparticles or cells translocate through a micro/nanosensing aperture, the aperture is electrically blocked because these nonconducting particles displace the conducting electrolyte solution. This results in significant electrical current change across the aperture. By analyzing the change of electrical pulse amplitude and pulse bandwidth, the information of size and numbers of the microparticles can be obtained. Recently, due to the fast development of micro/nanofabrication technology, micro-Coulter counters have been developed for point of care analysis of whole blood cells and cancer cells at low cost [1]. It is well known that the circulating tumor cells (CTCs) are shed from primary tumor and transported in circulatory blood to a distant organ forming metastasis, which is the major cause of mortality in most cancer patients. Since the number density of CTCs in blood is proportionally correlated to metastases, accurate enumeration of CTCs in the circulatory blood is critical for monitoring disease progression and assessing the patient response to treatment. However, it is of great challenge to detect and quantify the CTCs in the early cancer stage, which is due to the fact that the CTCs are extremely rare compared with other blood cells. There are many current methods for CTC detection using their unique physical properties, or fluorescent nanobioprobes based on the immunoreactions between the antibodies and the cancer biomarkers expressed on their cell surface [8], [9]. The conventional flow cytometry technique that is based on the fluorescent tag and laser optical detection is limited due to high operation cost and bulky instruments. Meanwhile, the microfluidic impedance cytometry can provide a rapid and less costly solution for the characterization of CTCs. The next generation of Coulter counters will have multiple channels which are expected to achieve much higher detection efficiency in a very short time. Therefore we present, in this paper, a numerical model for a comprehensive analysis of a microfluidic impedance flow cytometer for point of care CTC detection and enumeration.

Manuscript received February 14, 2013; revised May 8, 2013; accepted August 5, 2013. Date of publication August 15, 2013; date of current version November 18, 2013. The work of Y. Kang was supported by a start-up grant from the College of Engineering and Academic Research Fund, Nanyang Technological University, Ministry of Education of Singapore under Grant RG 26/11. The work of T. S. Pui and A. R. A. Rahman was supported by A*STAR under JCO Grant #11/3/06/ASC/02. The work of J. Guo was supported by the Ph.D. scholarship from Nanyang Technological University. *Asterisk indicates the corresponding author*.

J. Guo is with the School of Chemical and Biomedical Engineering, Nanyang Technological University, Singapore 637459 (e-mail: jguo002@e.ntu.edu.sg).

T. S. Pui and A. R. A. Rahman are with the A*STAR, Institute of Microelectronics, Singapore 117685 (e-mail: puits@ime.a-star.edu.sg; abdurr@ime.a-star.edu.sg).

Y.-L. Ban is with the Institute of Electromagnetics, University of Electronic Science and Technology of China, Chengdu 611731, China (e-mail: byl@uestc.edu.cn).

*Y. Kang is with the School of Chemical and Biomedical Engineering, Nanyang Technological University, Singapore 637459 (e-mail: yuejun.kang@ntu.edu.sg).

Color versions of one or more of the figures in this paper are available online at http://ieeexplore.ieee.org.

Digital Object Identifier 10.1109/TBME.2013.2278014

II. Theory and Method

A. Mathematical Theory

The structure of the microfluidic cytometer consists of four reservoirs (A, B, C, D). A/B are for sample inlet and outlet, respectively. C/D are the liquid channels that act as the conducting electrodes [see Fig. 1(a)]. The widths of the main channel and the conducting liquid channel are 160 and 300 μm, respectively [see Fig. 1(b)]. The length and width of the sensing aperture are 150 and 25 μm, respectively. The entire channel has the same height of 30 μm.

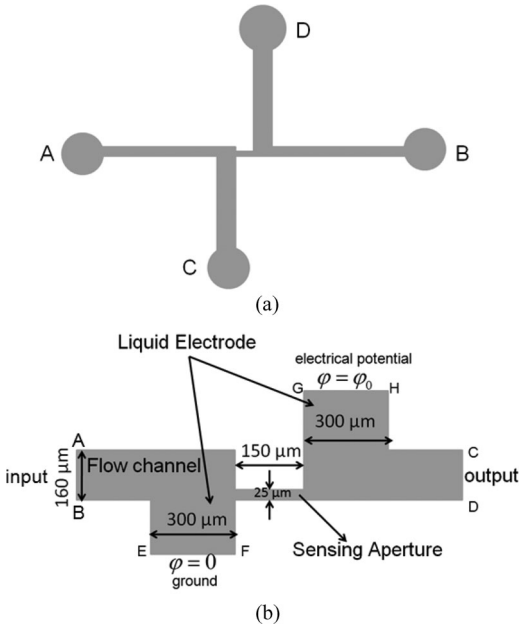

Fig. 1. (a) Schematic illustration of the microfluidic channel with four reservoirs; (b) central dimensions of the microfluidic channel.

As mentioned earlier, the particle translocates through the sensing aperture and results in an electric current change. A 3-D model is developed using commercial finite element method (FEM) software, COMSOL Multiphysics 4.3 (COMSOL, CA, USA). During the simulation, the particle is released at an upstream location that is 110 μm away from the entry of the sensing aperture to minimize the computation time without affecting the complete pulse profile before and after the particle translocates the aperture. This is because the channel resistance starts to change significantly only when the particle approaches very closely to the sensing aperture (within a distance equivalent to one or two particle diameters). The carrying liquid is driven by the inlet flow at channel entry, which exerts hydrodynamic force on the particle. The particle also experiences the electrophoretic and dielectrophoretic forces due to the electrical potential applied across the conducting liquid channel. In order to characterize the pulse profile resulted from particle translocation, all governing equations, including those for electrical field, flow field, and particle migration, need to be coupled together in computation. Both particle surface and channel walls are assumed nonconducting and rigid [10].

In addition to the FEM algorithm as used for this simulation, it is also worth noting that there are other computational fluid dynamics (CFD) methods for flow simulation. One of the popular approaches is Lattice Poisson–Boltzmann Method, which has been proved to be a very efficient scheme for 3-D simulation of electrohydrodynamic flows in micro- or nanoscale, especially for situations involving highly complex boundary conditions due to heterogeneous channel structure or surface charges [11], [12]. Since the proposed chip in this study has relatively simple structure and uniform surface conditions, the commercial FEM software package is accurate enough for the simulation purpose.

1) Electrical Field: In the computational domain in Fig. 1, the electrical current density $\overrightarrow{J}$ through the fluidic channel is given by Ohm's law

$$\overrightarrow{J} = \sigma \overrightarrow{E} \tag{1}$$

where $\overrightarrow{E}$ is the electric field and σ is the electrical conductivity of the fluid. The electrical potential φ satisfies Poisson's equation

$$-\nabla \cdot (\varepsilon_0 \varepsilon_r \nabla \varphi) = \rho_\nu \tag{2}$$

where

$$\overrightarrow{E} = -\nabla \varphi \tag{3}$$

ε_0 and ε_r are the permittivity of vacuum and the relative permittivity of the liquid, respectively. ρ_v is the space charge density. Since the electrolyte solution is neutral and the particle is assumed as nonconducting, there is no net charge in the whole computation domain, we can simplify the Poisson's equation as

$$-\nabla \cdot (\varepsilon_0 \varepsilon_r \nabla \varphi) = 0. \tag{4}$$

The boundary conditions are as follows.

Electrical potential at reservoir D [see Fig. 1(a)]

$$\varphi = 10 \text{ mV}. \tag{5a}$$

Grounded reservoir C [see Fig. 1(a)]

$$\varphi = 0 \text{ V}. \tag{5b}$$

Insulating channel walls and particle surface

$$\overrightarrow{n} \cdot \nabla \varphi = 0. \tag{5c}$$

The total electrical current is obtained by the integration of current density over any cross section of the channel

$$I = \iint_S \overrightarrow{J} \cdot d\overrightarrow{s} = \iint_S \sigma \frac{\partial \varphi}{\partial z} ds. \tag{6}$$

2) Flow Field: For the CFD module, the boundary condition at the channel wall is given by Smoluchowski formula assuming that the electrical double layer (EDL) is very thin compared to the channel size [13], [14]; at the particle surface, the boundary condition is given by combining the particle velocity with the electroosmotic flow velocity [14]. The governing equations are as follows.

Navier–Stokes equation

$$\rho \left[\frac{\partial \overrightarrow{u}}{\partial t} + \overrightarrow{u} \cdot \nabla \overrightarrow{u} \right] = -\nabla p + \mu \nabla^2 \overrightarrow{u}. \tag{7}$$

Continuity equation

$$\nabla \cdot \overrightarrow{u} = 0. \tag{8}$$

Boundary conditions are as follows.

Channel walls

$$\overrightarrow{u} = -\frac{\varepsilon_0 \varepsilon_r \zeta_w}{\mu} \overrightarrow{E}, \quad \overrightarrow{n} \cdot \nabla p = 0. \tag{9a}$$

Particle surface

$$\overrightarrow{u} = \overrightarrow{V_p} - \frac{\varepsilon_0 \varepsilon_r \zeta_p}{\mu} \overrightarrow{E}, \quad \overrightarrow{n} \cdot \nabla p = 0. \tag{9b}$$

Channel inlet

$$\overrightarrow{n} \cdot \nabla \overrightarrow{u} = 0, \quad v_{\text{inlet}} = v_0. \tag{9c}$$

Channel outlet

$$\overrightarrow{n} \cdot \nabla \overrightarrow{u} = 0, \quad p = 0 \tag{9d}$$

where $\overrightarrow{u}$ is flow field; v_0 denotes the inlet flow velocity; ρ is the fluid density; μ is the dynamic viscosity; ζ_p and ζ_w are zeta potentials at particle surface and channel wall, respectively; $\overrightarrow{V_p}$ is the translational velocity of the particle.

3) Particle Motion: Under the pressure-driven flow in the main channel (A–B) and the electrical potential applied across the side channel (C–D), the particle migration is due to the combination of hydrodynamic flow and electroosmotic flow. The particle also experiences the electrophoretic and dielectrophoretic forces due to the nonuniform electrical field in the aperture. The particle migration is described by Newton's second law

$$m_p \frac{d\overrightarrow{V_p}}{dt} = \overrightarrow{F}_{\text{net}} \tag{10}$$

where m_p is the particle mass; $\overrightarrow{V_p}$ is the translational velocity. The net force $\overrightarrow{F}_{\text{net}}$ consists of three components: electrophoretic force $\overrightarrow{F}_{EP}$ due to the applied electrical field, dielectrophoretic force $\overrightarrow{F}_{DEP}$ due to the nonuniform electrical field near/in the aperture, and the hydrodynamic force $\overrightarrow{F}_h$ due to the carrying flow field

$$\overrightarrow{F}_{\text{net}} = \overrightarrow{F}_{EP} + \overrightarrow{F}_{DEP} + \overrightarrow{F}_h. \tag{11}$$

The dielectrophoretic force can be evaluated by integrating the Maxwell stress tensor over the surface of the particle [15]

$$\overrightarrow{F}_{DEP} = \oint_S \overline{\overline{T}} \cdot \overrightarrow{n}\, dS \tag{12}$$

where $\overrightarrow{n}$ is the unit vector normal to the surface; and $\overline{\overline{T}}$ is the Maxwell stress tensor defined as (for static electric field)

$$\overline{\overline{T}} = \varepsilon \left(\overrightarrow{E} \otimes \overrightarrow{E} - \frac{1}{2} \overrightarrow{E}^2 \overline{\overline{I}} \right) \tag{13}$$

where $\overline{\overline{I}}$ is the unit tensor and symbol $\otimes$ denotes the dyadic product.

The flow field around the particle surface consists of two unique regions: inner region and outer region. Under the assumption of thin EDL with thickness characterized by Debye length [10], the electroosmotic flow exists on the surface of particle in the inner region. While in the outer region, the positive ions are neutralized by the negative ions that lead to the zero local volume charge density. Under this assumption, the hydrodynamic force $\overrightarrow{F}_h$ can be divided into two components

$$\overrightarrow{F}_h = \overrightarrow{F}_{ho} + \overrightarrow{F}_{hin} \tag{14}$$

where $\overrightarrow{F}_{hin}$ is due to the electroosmotic flow field in the inner region near the particle surface (within EDL), and $\overrightarrow{F}_{ho}$ is resulted from the flow field in the outer region. In this situation, the EDL thickness is of nanometer scale and much thinner compared to micron scale of particle size. In addition, $\overrightarrow{F}_{hin}$ and $\overrightarrow{F}_{EP}$ have the same magnitude but act in opposite directions, which implies they are counterbalanced in (11) [16]. Therefore, the net force acting on the particle reduces to

$$\overrightarrow{F}_{\text{net}} = \overrightarrow{F}_{DEP} + \overrightarrow{F}_{ho}. \tag{15}$$

In this equation, the hydrodynamic force in the outer region is described by integrating the hydrodynamic stress tensor over the particle surface [14], [16]

$$\overrightarrow{F}_{ho} = -\oiint_S \overline{\overline{\sigma}}_p \cdot \overrightarrow{n}\, dS \tag{16}$$

where the hydrodynamic stress tensor $\overline{\overline{\sigma}}$ is defined as

$$\overline{\overline{\sigma}} = -p\overline{\overline{I}} + \mu \left[\nabla \overrightarrow{u} + (\nabla \overrightarrow{u})^T \right]. \tag{17}$$

For simplicity, the initial velocity of particle motion in (10) is set as zero

$$\overrightarrow{V_p}\,|_{t=0} = 0 \quad \overrightarrow{u}\,|_{t=0} = 0\,. \tag{18}$$

The Joule heating effect on the electrokinetic motion of the particles is neglected during the simulation due to the fact that very low dc voltage (10 mV) is applied across the side channel. In the simulation, the average electric field strength through the entire side channel is numerically calculated as 0.01 V/cm, which is far below the threshold field strength 200 V/cm for obvious Joule heating effect [17]. Therefore, this assumption is valid.

B. Numerical Simulation

In the multiphysical modeling, the boundary at the particle surface is not static but time dependent because the particle keeps moving in the channel. COMSOL 4.3 and MATLAB R2011b (Mathworks, MA, USA) are combined to conduct the real-time numerical simulation. The FEM model comprises total of 870 290 elements after refined meshing. The COMSOL dc and CFD modules can compute transient values of the parameters including flow field and electrical field, which are postprocessed to compute the net force acting on the particle. These parameters are imported into MATLAB by an interface with COMSOL to calculate the displacement of the particle by the next time loop. The displacement and velocity of particle are stored by MATLAB and updated to COMSOL through the same interface. COMSOL can regenerate the updated model and compute the new flow field and electrical field. The computation loop is coded in MATLAB to manage the whole progress. The major constants in the numerical modeling are listed in Table I.

C. Method

1) Device Fabrication: The soft-lithography technique was used to pattern the microfluidic channel. Negative photoresist SU-8 (SU-8 3050, Microchem, MA, USA) was spin-coated on a glass slide and soft baked (65 °C for 5 min, 95 °C for 15 min). After UV light exposure for 20 s and postbaking (65°C for 1 min, 95 °C for 5 min), the SU-8 mold with thickness of 30 μm was developed on a clean glass slide. The PDMS (Sylgard 184, Dow Corning, MI, USA) and curing agent with a volume ratio of 10:1 were then mixed together and cast onto the SU-8 mold.

TABLE I
MAJOR CONSTANTS IN NUMERICAL SIMULATION

Relative permittivity of fluid ε_r	80
Permittivity of vacuum ε_0 (C/Vm)	8.854×10^{-12}
Viscosity of fluid μ (kg/ms)	0.9×10^{-3}
Density of fluid ρ (kg/m^3)	998
Electric conductivity of fluid σ (S/m)	1.6
Zeta potential on particle surface ξ_p (mV) [18]	-40
Zeta potential on channel wall ξ_w (mV) [19]	-50
Aperture width D (μm)	25
Aperture length L (μm)	150
Channel height H (μm)	30
Particle diameter d (μm)	5, 16

The fluid properties is based on 1X PBS solution at 20°C.

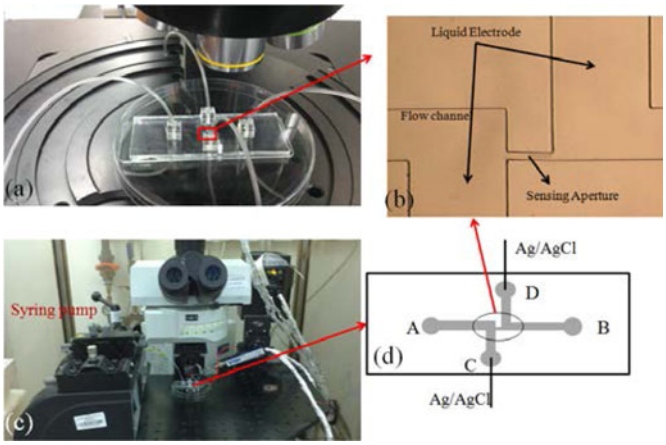

Fig. 2. (a) Microfluidic chip and tubing; (b) Microscopic image of the central chip structure; (c) Experimental setup for observation and electrical measurement by a patch clamp; (d) Schematic illustration of the whole chip.

After degassing in a vacuum box, the PDMS was moved into an oven and cured at 75 °C for 2 h. Finally, the PDMS replica was peeled off from the mold and bonded to a clean glass substrate by plasma treating for 10 s.

2) Cell Culture: Breast cancer cells MCF-7 (American Type Culture Collection, MD, USA) derived from breast adenocarcinoma were cultured in Minimum Essential Media (MEM) (Gibco, cat# 11095-080) supplemented with 10% fetal bovine serum (FBS) (Gibco, cat# 10270106), 1 mM sodium pyruvate (Gibco, cat# 11360-070), and 0.1 mM MEM nonessential amino acids (Gibco, cat# 11140-050), and grown at 37 °C under 5% CO_2 atmosphere in a T75 flask. For flow testing, low concentration of MCF-7 cells (1×10^4 cell/mL) spiked in 1X PBS (Sigma-Aldrich, St. Louis, MO, USA) were injected through the inlet channel A.

3) Measurement Setup: Fig. 2 shows the typical measurement setup. The device was positioned on a microscope stage that was housed in a Faraday cage. Two Ag/AgCl electrodes were inserted into two reservoirs, C and D, respectively. 1X PBS buffer solution was used as the carrier fluids for polystyrene particles and tumor cells. The electrical current of the sensing channel was measured under a bias of 10 mV using HEKA patch clamp amplifier (HEKA Electronik, Lambrecht, Germany) and the data were imported into a homemade MATLAB (Mathworks, MA, USA) program for postprocessing.

III. RESULTS AND DISCUSSION

A. Translocation Simulation

In this section, we present the simulation results of the particle velocity profile under the hydrodynamic and electrokinetic forces. The translocation time was simulated under the effect of different particle sizes (5 and 16 μm).

The modulation of electrical pulse amplitude due to the blockage by the particles has been investigated in other studies [20]–[23]. In this simulation, however, we emphasize the electrical pulse bandwidth that corresponds to the total time duration when the particle is present in the sensing aperture, which has rarely been studied in the previous research. Generally, the translocation time mainly depends on the flow rate that carries the particle through the aperture. Since the fluid flow is mainly pressure driven, the applied pressure across the channel determines the flow rate. Fig. 3(a) shows the velocity profile and translocation time of a 5 μm polystyrene particle under the inlet flow rate of 1.5 μL/min and 10 mV electrical bias and Fig. 3(b) shows the velocity profile under the same flow rate for a 16 μm polystyrene particle. It can be seen that the velocity modulation becomes narrower and the equilibrium translocation velocity has higher magnitude when the particle size decreases.

The simulation showed that the electrokinetic force is three orders of magnitude lower than the hydrodynamic force and thus can be neglected. If the particle radius is denoted as r, the hydrodynamic force is proportional to the particle surface area $F_h \propto r^2$; the particle mass is proportional to its volume $m \propto r^3$; thus the particle acceleration is proportional to the scale of r^{-1}, which predicts that a smaller particle accelerates faster than a larger particle. As Fig. 3 shows that the acceleration time for a 5 μm particle is around 0.125 ms, while the acceleration time is around 0.25 ms for a 16 μm particle. The simulation showed a similar trend as predicted by above theoretical analysis. In addition, the equilibrium velocity for a 5 μm particle is 0.093 m/s, which is higher than the equilibrium velocity 0.078 m/s for the 16 μm particle. This might explain why the translocation time of a 16 μm particle is longer than that of a 5 μm particle. This feature can help distinguish signals, for example, induced by red blood cells from those by tumor cells and verify if the signal is caused by a single cell or assembly of multiple cells. To further validate the simulation, we conducted the experiment and compared the simulation results with the experimental data obtained for 5 and 16 μm polystyrene particles, and tumor cells that have an average size of 16 μm.

B. Experimental Results

The 5 and 16 μm polystyrene particles and breast cancer cells (16 μm in average) are suspended in 1X PBS buffer and introduced to the microchannel at a flow rate of 1.5 μL/min. The electrical bias cross the sensing channel is set to 10 mV and the electrical signal is recorded by a patch clamp system. Fig. 4(a) and (b) shows both experimental and simulated electrical pulses induced by a single 5 and a 16 μm polystyrene particle, respectively. The electrical current for 5 μm particle drops by around 17.7 nA and the pulse bandwidth is 1.93 ms;

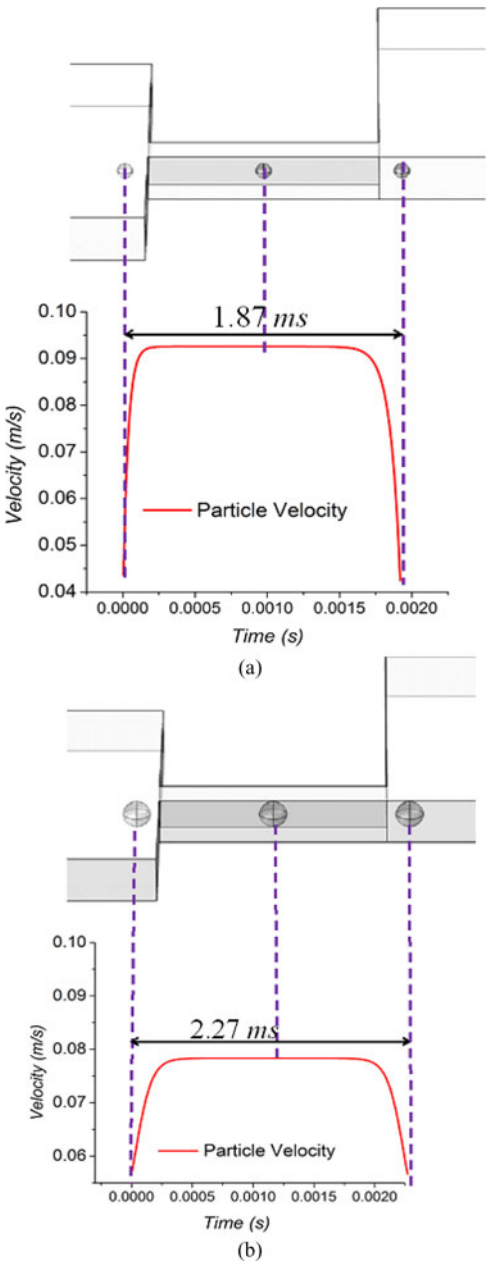

Fig. 3. Particle velocity change during translocation through the sensing aperture: (a) velocity profile and translocation time for a 5 μm particle; (b) velocity profile and translocation time for a 16 μm particle.

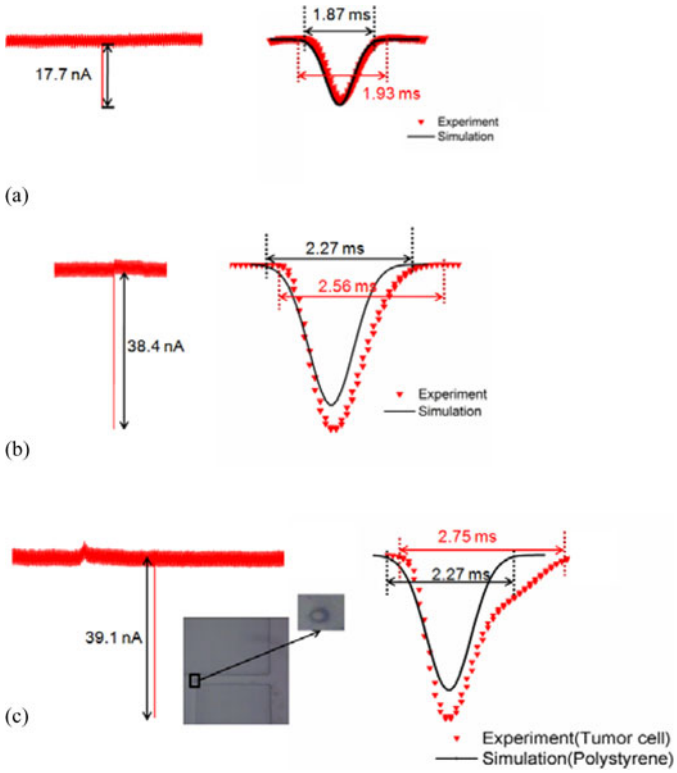

Fig. 4. Measured electrical pulses caused by a 5 μm (a) and a 16 μm (b) polystyrene particles, compared with the simulation results; (c) measured electrical pulse caused by a breast cancer cell compared with the simulated result for a polystyrene particle of the same size (16 μm in diameter).

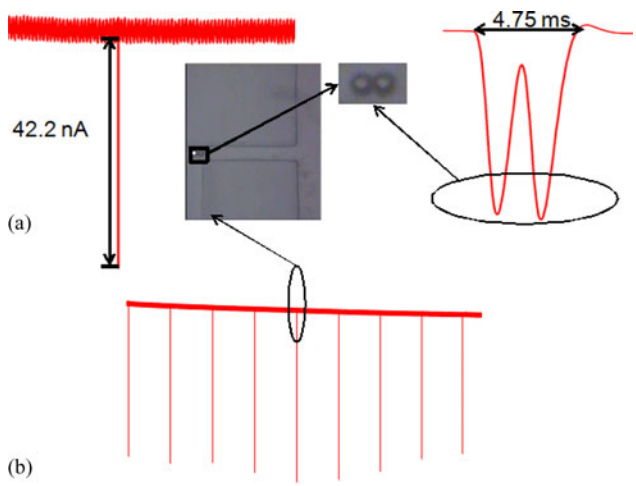

Fig. 5. (a) Electrical pulse profile caused by aggregation of two breast cancer cells; (b) Continuous electrical pulse profile of many breast cancer cells.

while for the 16 μm particle, the pulse amplitude is 38.4 nA and the bandwidth is 2.56 ms, both showing good agreement with the simulation results. Fig. 4(c) shows the measured pulse profile for a single breast cancer cell, which has pulse amplitude of 39.1 nA and bandwidth of 2.75 ms. We also compared this pulse profile of the tumor cell with the simulation result for a polystyrene particle of the same size (16 μm). The asymmetric profile of the measured pulse in Fig. 4(c) might be attributed to the deformation of the tumor cell in the narrow sensing aperture, which was not considered in the current numerical modeling.

In the experiment, assemblies of multiple particles sticking together while transporting in the sensing aperture were detected by both electrical method and optical microscopy. Fig. 5(b) shows a continuous electric pulse profile for many breast cancer cells suspended in sample fluid. Among these pulses, some demonstrate prolonged bandwidth while the amplitude remains the same. By examining these abnormal pulses in detail such as the one in Fig. 5(a), we can identify that each of these pulses actually includes two sharp peaks. With concurrent microscopic visualization, we have verified that these abnormal pulses are caused by an aggregation of twin particles, which depart from

each other but still move closely during translocation through the sensing aperture. The bandwidth in Fig. 5(a) is 4.75 ms, which is roughly two times of the bandwidth in Fig. 4(c) for a single tumor cell. Each of these two similar peaks corresponds to the incidence of every single particle. This abnormal pulse profile is in a good agreement with the numerical simulation in the authors' previous work [13]. This finding implies that, solely relying on the measured pulse amplitude, it is hard to determine the exact number of the particles during translocation through the sensing aperture. However, the pulse bandwidth that corresponds to the translocation time is another critical parameter for accurate particle enumeration.

IV. Conclusion

In this paper, we present a numerical model for the systematic analysis of a micro-Coulter counter for point of care diagnosis, which can concurrently characterize both electric current amplitude and bandwidth. The polystyrene particles and breast cancer cells are tested in the fabricated device to demonstrate the accuracy of this model. The experimental results show that the model can make a good prediction on enumeration of cell events by determining the translocation time. In general, this model can provide critical insight and guidance for developing the new micro-Coulter counter for low cost and rapid detection and enumeration of rare cells.

Acknowledgment

The authors declare no financial or commercial conflicts of interest.

References

[1] W. Asghar, Y. Wan, A. Ilyas, R. Bachoo, Y. T. Kim, and S. M. Iqbal, "Electrical fingerprinting, 3D profiling and detection of tumor cells with solid-state micropores," *Lab Chip*, vol. 12, no. 13, pp. 2345–2352, 2012.

[2] A. V. Jagtiani, J. Zhe, J. Hu, and J. Carletta, "Detection and counting of micro-scale particles and pollen using a multi-aperture coulter counter," *Meas. Sci. Technol.*, vol. 17, no. 7, pp. 1706–1714, 2006.

[3] S. Zheng, M. Liu, and Y. C. Tai, "Micro coulter counters with platinum black electroplated electrodes for human blood cell sensing," *Biomed. Microdevices*, vol. 10, no. 2, pp. 221–31, 2008.

[4] Y. Wu, D. B. James, and A. Mahmoud, "Micromachined coulter counter for dynamic impedance study of time sensitive cells," *Biomed. Microdevice*, vol. 14, no. 4, pp. 739–750, 2012.

[5] I. Z. Jeffrey, "Impedance-based flow cytometry for the measurement of microparticles," *Semin. Thromb. Hemost.*, vol. 36, no. 8, pp. 819–823, 2010.

[6] J. S. Lorenz, O. Oliver, C. Catalin, G. Joanne, and F. K. Ulrich, "Detecting DNA folding with nanocapillaries," *Nano Lett.*, vol. 10, no. 7, pp. 2493–2497, 2010.

[7] H. Bayley and C. R. Martin, "Resistive-pulse sensing-from microbes to molecules," *Chem. Rev.*, vol. 100, no. 7, pp. 2575–2594, 2000.

[8] M. Yu, S. Stott, M. Toner, S. Maheswaran, and D. A. Haber, "Circulating tumor cells: Approaches to isolation and characterization," *J. Cell Biol.*, vol. 192, no. 3, pp. 373–382, 2011.

[9] P. Paterlini-Brechot and N. L. Benali, "Circulating tumor cells detection: Clinical impact and future directions," *Cancer Lett.*, vol. 253, no. 2, pp. 180–204, 2007.

[10] Y. Kang and D. Li, "Electrokinetic motion of particles and cells in microchannels," *Microfluidics Nanofluidics*, vol. 6, no. 4, pp. 431–460, 2009.

[11] J. Wang, M. Wang, and Z. Li, "Lattice Poisson–Boltzmann simulations of electro-osmotic flows in microchannels," *J. Colloid Interface Sci.*, vol. 296, no. 2, pp. 729–736, 2006.

[12] M. Wang, N. Pan, J. Wang, and S. Chen, "Lattice Poisson–Boltzmann simulations of electroosmotic flows in charged anisotropic porous media," *Commun. Comput. Phys.*, vol. 2, no. 6, pp. 1055–1070, 2007.

[13] J. Guo, T. S. Pui, A. R. A. Rahman, and Y. Kang, "3D numerical simulation of a coulter counter array with analysis of electrokinetic forces," *Electrophoresis*, vol. 34, no. 3, pp. 417–424, 2013.

[14] Z. Wu, Y. Gao, and D. Li, "Electrophoretic motion of ideally polarizable particles in a microchannel," *Electrophoresis*, vol. 30, no. 5, pp. 773–781, 2009.

[15] B. Cetin and D. Li, "Dielectrophoresis in microfluidics technology," *Electrophoresis*, vol. 32, no. 18, pp. 2410–2427, 2011.

[16] C. Ye and D. Li, "3-D transient electrophoretic motion of a spherical particle in a T-shaped rectangular microchannel," *J. Colloid Interface Sci.*, vol. 272, no. 2, pp. 480–488, 2004.

[17] J. Zhu, S. Sridharan, G. Hu, and X. Xuan, "Joule heating effects on electrokinetic focusing and trapping of particles in constriction microchannels," *J. Mciromech. Microeng.*, vol. 22, no. 7, p. 075011, 2012.

[18] P. H. Thonart, M. Custinne, and M. Paquot, "Zeta potential of yeast cells: Application in cell immobilization," *Enzyme Microbiol. Technol.*, vol. 4, no. 3, pp. 191–194, 1982.

[19] B. J. Kirby and E. F. Hasselbrink, "The zeta potential of microfluidic substrates—Part 1: Theory, experimental techniques, and effects on separations," *Electrophoresis*, vol. 25, no. 2, pp. 187–202, 2004.

[20] J. C. Maxwell, *A Treatise on Electricity and Magnetism*. New York, NY, USA: Dover, 1991.

[21] R. W. DeBlois, C. P. Bean, and R. K. A. Wesley, "Electrokinetic measurements with submicron particles and pores by the resistive pulse technique," *J. Colloid Interface Sci.*, vol. 61, no. 2, pp. 323–335, 1977.

[22] E. C. Gregg and K. D. Steidley, "Electrical counting and sizing of mammalian cells in suspension," *Biophys. J.*, vol. 5, no. 4, pp. 393–405, 1965.

[23] Z. Qin, J. Zhe, and G. X. Wang, "Effects of particle's off-axis position, shape, orientation and entry position on resistance changes of micro coulter counting devices," *Meas. Sci. Technol.*, vol. 22, no. 4, p. 045804, 2011.

Jinhong Guo received the B.E. degree in electronic engineering in 2010 from the University of Electronic Science and Technology of China, Sichuan, China. Currently, he is working toward the Ph.D. degree at Nanyang Technological University (NTU) jointly attached to Institute of Microelectronics, A*STAR, Singapore.

Before joining the Applied Microfluidicology Lab, NTU, he worked as a Research Engineer for RFIC design at VIRTUS Integrated Circuit Design Lab in NTU until August 2011. His research interests include micro/nanosolid-state biosensor, microfluidic electronics, optofluidic sensor, microwave-driven microfluidics, and nanoelectromagnetics.

Tze Sian Pui received the M.Sc. degree in medical physics from the University of Malaya, Kuala Lumpur, Malaysia, in 2004, and the Ph.D. degree in biomedical engineering from the Nanyang Technological University, Singapore, in 2011.

Currently, he is a Scientist at the Institute of Microelectronics, A*STAR, Singapore. His research interests include high throughput, high content screening systems for biological analysis, and electrical/electrochemical assays for cell-based biosensing.

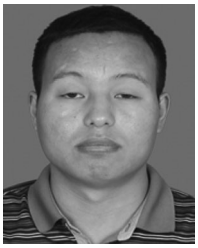

Yong-Ling Ban received the B.S. degree in mathematics from Shandong University, Shandong, China, the M.S. degree in electromagnetics from Peking University, Beijing, China, and the Ph.D. degree in microwave engineering from University of Electronic Science and Technology of China (UESTC), Sichuan, China, in 2000, 2003, and 2006, respectively.

In July 2006, he joined the Institute of Xi'an Mechanical and Electrical Information from China North Industries Group Corporation as a Microwave Engineer. Later, he moved to Huawei Technologies Company, Ltd., Shenzhen, first as a RF Antenna Design Engineer and then as a Senior Design Engineer. In Huawei, he designed and implemented various antennas for 15 data card and mobile phone products customized from leading telecommunication industries like Vodafone. From August 2010 to present, he has been as an Associate Professor at the Department of Microwave Engineering from UESTC. His research and development interests include wideband small antenna for 3G/LTE handheld and mobile devices, directional patch antennas and arrays for mobile small base station, MIMO antenna decoupling techniques, and nanoantenna.

Abdur Rub Abdur Rahman received the Ph.D. degree from the University of South Florida, FL, USA, in 2007. He received the M.Sc. degree in MEMS from the University of Cincinnati, OH, USA, in 2000.

Before Ph.D. he served as a MEMS Process Development Engineer at Formfactor, Inc., and Standard MEMS, Inc., between the years 2000 and 2002. He is a Principal Investigator in the Bioelectronics Department, Institute of Microelectronics, A*STAR, Singapore. His research interests include development and commercialization of *in vitro* clinical diagnostic systems.

Yuejun Kang received the Ph.D. degree in mechanical engineering from Vanderbilt University, Tennessee, USA, in 2008 and Nanyang Technological University (NTU), in 2005, respectively.

Before joining the School of Chemical Biomedical Engineering, NTU, as an Assistant Professor in late March 2011, he worked as a Postdoctoral Researcher in Monash University and Los Alamos National Laboratory. His research interests include fundamental understanding of micro/nanofluidics, and leverage these understanding toward the frontier lab-on-a-chip technologies to address critical and challenging questions in diagnostics, therapeutics, tissue engineering, and regenerative medicine, as well as bioenergy and environmental studies. His current research focus includes microfluidic biosensors and environmental sensors, cells-on-a-chip, on-chip tissue engineering, and therapeutic microdevices.